CHEMISTRY
A EUROPEAN JOURNAL

DOI: 10.1002/chem.200800394

Structures and Solvatochromic Phosphorescence of Dicationic Terpyridyl–Platinum(II) Complexes with Foldable Oligo(*ortho*-phenyleneethynylene) Bridging Ligands

Ming-Xin Zhu, Wei Lu, Nianyong Zhu, and Chi-Ming Che*[a]

Abstract: A series of binuclear organoplatinum(II) complexes, $[(t\mathrm{Bu_3tpy})\mathrm{Pt}-(\mathrm{C}\equiv\mathrm{C}-1,2\text{-}\mathrm{C_6H_4})_n-\mathrm{C}\equiv\mathrm{C}-\mathrm{Pt}(t\mathrm{Bu_3tpy})][\mathrm{ClO_4}]_2$ (**1**–**7**, $n=1$, 2, 3, 4, 5, 6, 8; $t\mathrm{Bu_3tpy}$ = 4,4′,4″-tri-*tert*-butyl-2,2′:6′,2″-terpyridine) with foldable oligo(*ortho*-phenyleneethynylene) linkers were prepared and characterized by spectroscopic methods and/or X-ray crystallographic analyses. In the crystal structures of **3**·2.5 $\mathrm{CH_3OH}$, **5**·$\mathrm{CH_3CN}$, and **6**·4 $\mathrm{CH_3CN}$, each of the bridging *ortho*-phenyleneethynylene ligands has a partially folded conformation. In aerated water/acetonitrile mixtures with water percentages larger than 40%, the emission of complexes **3**–**7** are red-shifted and enhanced when compared to those recorded in acetonitrile. The red-shift in emission energy and enhanced emission intensity can be attributed to the inter- and/or intramolecular interactions induced by the addition of water to solutions of the platinum(II) complexes in acetonitrile. Data from dynamic light scattering and transmission electron microscopy studies revealed that these binuclear platinum(II) complexes aggregated into nanosized particles in acetonitrile/water mixtures. Hydrophobic folding of the *ortho*-phenyleneethynylene linkers in acetonitrile/water mixtures is postulated.

Keywords: aggregation · hydrophobic effect · luminescence · phenyleneethynylene · platinum

Introduction

Phosphorescent transition-metal complexes are useful optoelectronic[1] and chemosensory[2] materials. Of particular interest are those metal complexes supported by alkynyl ligands that have received much attention in recent years.[3] Alkynyl ligands are strong σ-donors, destabilize the HOMO of metal ions, and consequently suppress the nonradiative d–d state deactivation, resulting in high emission quantum yields and long emission lifetimes.[3c,d] In this regard, platinum(II)–terpyridyl complexes containing alkynyl ligands are particularly attractive, since they possess rich photophysical and spectroscopic properties, For example, the $[(\mathrm{tpy})\mathrm{Pt}(\mathrm{C}\equiv\mathrm{CAr})]^+$ (tpy = 2,2′:6′,2″-terpyridine) complexes have been demonstrated to have long-lived triplet metal-to-ligand charge-transfer (MLCT) and/or triplet ligand-to-ligand charge-transfer (LLCT) excited states.[4] Due to the square-planar geometry of platinum(II) complexes, their emissive triplet excited states are usually influenced by intra- and intermolecular interactions, including Pt···Pt and π–π interactions, which are sensitive to solvent composition, complex concentration and nucleophiles.[5] Subtle variations in the coordination sphere and the microenvironment of the platinum(II) complexes could lead to remarkable fluctuations in both their supramolecular structures and spectroscopic properties. Recent developments in phosphorescent organogelators derived from terpyridyl–platinum(II)–acetylide complexes are examples of the above perspective.[6]

Poly(phenyleneethynylene)s are a class of carbon-rich materials with extended π conjugations and have received considerable attention in materials chemistry.[7] When compared to the rigid linear oligo(*para*-phenyleneethynylene) (*para*-PE) compounds, oligo(*meta*-phenyleneethynylene) (*meta*-PE) and oligo(*ortho*-phenyleneethynylene) (*ortho*-PE) analogues each have a flexible, angular configuration that would allow the occurrence of a folded helical conformation with the repeating unit of six and three aryl rings, respectively.[8] It is anticipated that the folding of angular *meta*- and *ortho*-PEs would be affected by solvent, temperature, hydrogen bonding and metal-ion coordination.[9] Thus *meta*- and *ortho*-PEs could be useful linkers to construct phosphor-

[a] M.-X. Zhu, Dr. W. Lu, Dr. N. Zhu, Prof. Dr. C.-M. Che
Department of Chemistry and
Open Laboratory of Chemical Biology of the
Institute of Molecular Technology for Drug Discovery and Synthesis
The University of Hong Kong, Pokfulam Road, Hong Kong (China)
Fax: (+852) 2857-1586
E-mail: cmche@hku.hk

Supporting information for this article is available on the WWW under http://dx.doi.org/10.1002/chem.200800394.

escent metal–organic systems with folding properties arising from π–π stacking and solvophobic interactions in solution. Despite the extensive coordination chemistry of *meta*- and *para*-PE ligands, metal complexes with *ortho*-PE ligands are sparse in the literature.[10] Herein, we report the uniquely red-shifted and enhanced phosphorescence of dicationic terpyridyl–platinum(II) complexes containing *ortho*-PE bridges, $[(t\mathrm{Bu_3tpy})\mathrm{Pt}{-}(\mathrm{C{\equiv}C{-}1,2\text{-}C_6H_4})_n{-}\mathrm{C{\equiv}C{-}Pt}(t\mathrm{Bu_3tpy})][\mathrm{ClO_4}]_2$ (**1**–**7**, $n=1$, 2, 3, 4, 5, 6, 8; $t\mathrm{Bu_3tpy}=4,4',4''$-tri-*tert*-butyl-2,2′:6′,2″-terpyridine), in aqueous medium. Two mononuclear complexes $[(t\mathrm{Bu_3tpy})\mathrm{Pt}{-}\mathrm{C{\equiv}CC_6H_5}]\mathrm{ClO_4}$ (**8**) and $[(t\mathrm{Bu_3tpy})\mathrm{Pt}{-}(\mathrm{C{\equiv}C\text{-}1,2\text{-}C_6H_4})_2\text{-}\mathrm{C{\equiv}CC_6H_5}]\mathrm{ClO_4}$ (**9**) were studied for comparison.

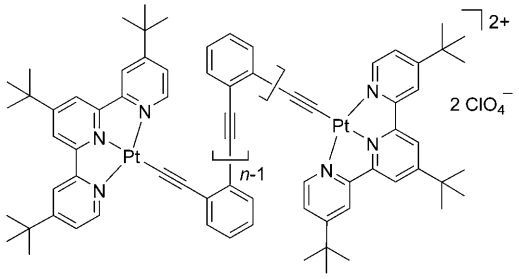

n = 1 (**1**), 2 (**2**), 3 (**3**), 4 (**4**), 5 (**5**), 6 (**6**), 8 (**7**)

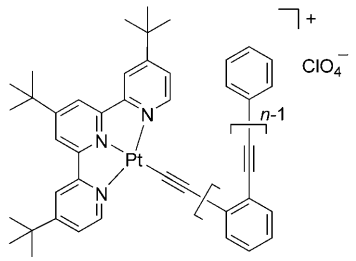

n = 1 (**8**), 3 (**9**)

Results

Synthesis and characterization: The series of terpyridyl–platinum(II) complexes (**1**–**8**) and **9** were synthesized through Sonogashira coupling reactions between $[(t\mathrm{Bu_3tpy})\mathrm{PtCl}]\mathrm{ClO_4}$ and the corresponding *ortho*-PEs (Scheme 1). For complexes **1**–**7**, the molar ratios of $[(t\mathrm{Bu_3tpy})\mathrm{PtCl}]\mathrm{ClO_4}$ to the $[\mathit{ortho}\text{-PE}(n)]\mathrm{H_2}$ ($\mathit{ortho}\text{-PE}(n)=\mathrm{C{\equiv}C{-}1,2\text{-}C_6H_4{-}(C{\equiv}C{-}1,2\text{-}C_6H_4)_{n-1}{-}C{\equiv}C}$, where $n=1$, 2, 3, 4, 5, 6, and 8, respectively) are 2:1; whereas for the mononuclear complexes **8** and **9**, the molar ratios of $((t\mathrm{Bu_3tpy})\mathrm{PtCl}]\mathrm{ClO_4}$ to the alkynyl ligand [$\mathrm{HC{\equiv}CC_6H_5}$ and $\mathrm{H(C{\equiv}C{-}1,2\text{-}C_6H_4)_2C{\equiv}CC_6H_5}$, respectively) are 1:1. Purification over a neutral $\mathrm{Al_2O_3}$ column with $\mathrm{CH_2Cl_2}$/acetone (volume ratio 4:1) followed by $\mathrm{CH_2Cl_2}$/$\mathrm{CH_3OH}$ (volume ratio 4:1) as eluents gave **1**–**9** as an orange or a red solid in moderate to high yields. The highest product yield was 90% (**8**) and the lowest was 47% (**5**). These complexes are air stable and soluble in $\mathrm{CH_2Cl_2}$, $\mathrm{CHCl_3}$, $\mathrm{CH_3CN}$, and acetone and slightly soluble in $\mathrm{CH_3OH}$. They were characterized by ^{1}H and ^{13}C NMR spectroscopy, and fast atom-bombardment (FAB) mass spectrometry (MS, see Experimental Section). As revealed by the ^{1}H NMR spectra of these complexes, the 2 and 6″ protons of the terpyridyl ligand appear as a doublet with two Pt satellites ($^3J_{\mathrm{PtH}}=\approx 40$ Hz), which was previously reported for terpyridyl–platinum(II) systems.[4,5] The FAB mass spectra of **1**–**7** reveal two major peaks corresponding to $[M-\mathrm{ClO_4}]^+$ and $[M-2\,\mathrm{ClO_4}]^+$, in which M represents the intact ion pair.

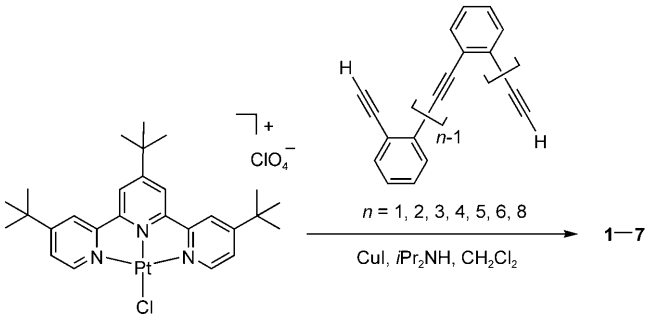

Scheme 1. Syntheses of complexes **1**–**7**.

X-ray crystallography: Crystals of $\mathbf{3}\cdot 2.5\,\mathrm{CH_3OH}$, $\mathbf{5}\cdot\mathrm{CH_3CN}$, and $\mathbf{6}\cdot 4\,\mathrm{CH_3CN}$ were obtained by slow diffusion of $\mathrm{Et_2O}$ into a solution of **3** in $\mathrm{CH_3OH}$ or solutions of **5** and **6** in $\mathrm{CH_3CN}$, and the crystal structures (Figure 1) were determined by X-ray crystal analysis. Crystallographic data collection parameters are summarized in Table 1. The Pt–C (1.94–1.99 Å) and C≡C (1.14–1.22 Å) bond lengths and Pt–C≡C (170.0–178.1°) and C–C≡C (172.4-178.9°) angles are comparable to those of reported platinum(II)–σ-alkynyl complexes containing terpyridyl and/or cyclometalated ligands.[4–5]

The crystal structure of **3** (Figure 1, left) shows that two $[(t\mathrm{Bu_3tpy})\mathrm{Pt}]$ moieties adopt a distorted planar geometry and are linked to each other by *ortho*-PE(3) through Pt–C bonds. The terpyridyl–platinum(II) planes and the phenyl rings of the bridging *ortho*-PE(3) fold into a two-layered helix as a result of the angular shape of the *ortho*-PE(3) units and the π–π interactions between the $[(t\mathrm{Bu_3tpy})\mathrm{Pt}]$ planes and their adjacent phenyl rings with interplanar distances of around 3.4 Å. Two $[(t\mathrm{Bu_3tpy})\mathrm{Pt}]$ planes in the same molecule have a dihedral angle of 26°. The view along the folding axis of the *ortho*-PE(3) moiety is close to a regular triangle. Despite the bulky *tert*-butyl groups at the periphery of terpyridyl ligand, there is a close intermolecular Pt···Pt contact (distance 3.24 Å) between two pairing cations in a head-to-tail fashion. These cation pairs are packed into infinite columns in the crystal structure. The intermolecular and interplanar distance between two neighboring terpyridyl planes is around 3.4 Å, which would allow for π–π interactions.

Each of the cations in **5** (Figure 1, middle) and **6** (Figure 1, right) folds into a three-layered sandwichlike structure with two terpyridyl–platinum(II) planes, one serves as the first and the other one as the third layer, while

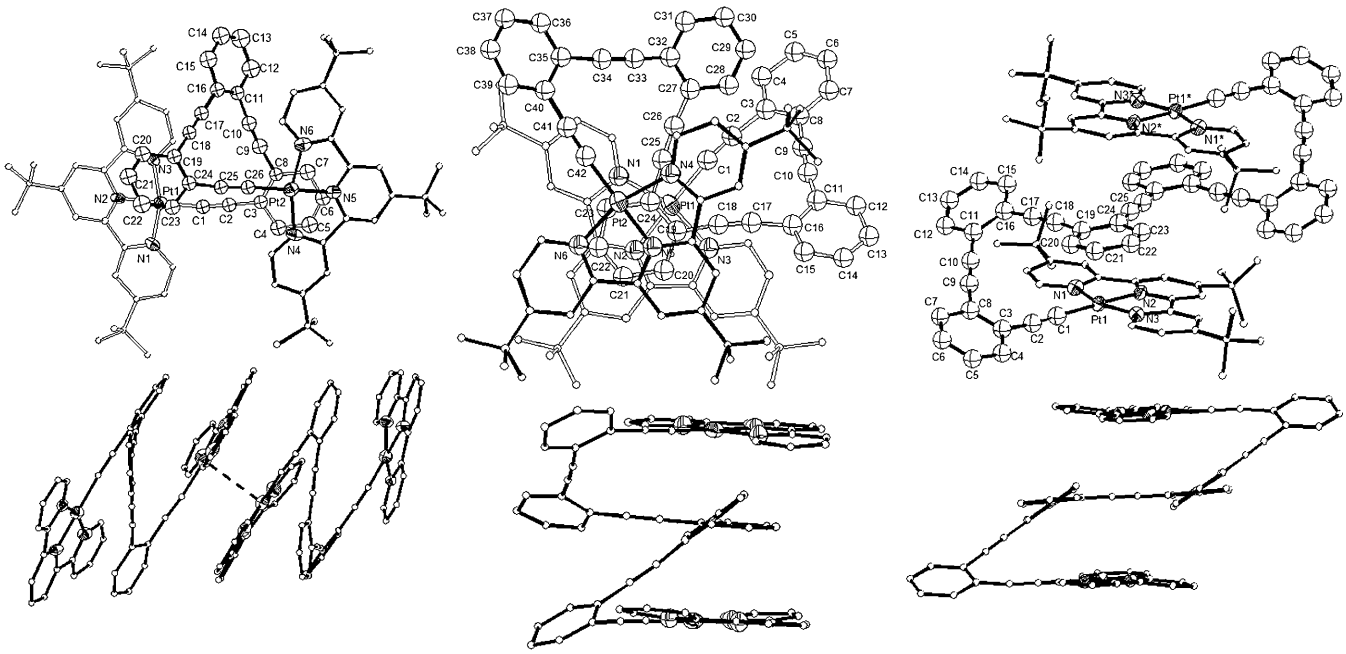

Figure 1. Left: Perspective view (top) of the cation in **3**·2.5 CH_3OH with hydrogen atoms, perchlorate ions and solvated molecules omitted for clarity. The side view (bottom) of the cations is shown to emphasize the conformation of the *ortho*-PE(3) bridges and the intramolecular folding through intramolecular π-π interactions and intermolecular Pt···Pt contacts (as indicated with dashed lines). Middle: Perspective view (top) and side view (bottom) of the cation in **5**·CH_3CN with hydrogen atoms, perchlorate ions and solvated molecules omitted for clarity. Right: Perspective view (top) and side view (bottom) of the cation in **6**·4 CH_3CN with hydrogen atoms, perchlorate ions and solvated molecules omitted for clarity.

Table 1. Crystal data of complexes **3**·2.5 CH_3OH, **5**·CH_3CN, and **6**·4 CH_3CN.

	3·2.5 CH_3OH	**5**·CH_3CN	**6**·4 CH_3CN
formula	$C_{82.5}H_{92}Cl_2N_6O_{10.5}Pt_2$	$C_{98}H_{93}Cl_2N_7O_8Pt_2$	$C_{112}H_{106}Cl_2N_{10}O_8Pt_2$
M_r	1796.70	1954.85	2181.15
color	red	orange red	orange
T [K]	253	301	253
crystal size [mm]	0.35×0.15×0.1	0.7×0.15×0.1	0.3×0.3×0.1
crystal system	monoclinic	monoclinic	triclinic
space group	$C2/c$	$P2_1/c$	$P\bar{1}$
a [Å]	28.180(6)	17.777(4)	17.444(4)
b [Å]	28.678(6)	30.505(6)	17.535(4)
c [Å]	19.779(4)	20.462(4)	19.790(4)
α [°]			78.05(3)
β [°]	90.10(3)	112.78(3)	69.92(3)
γ [°]			66.03(3)
V [Å^3]	15984(6)	10231(4)	5179(2)
Z	8	4	2
ρ_{calcd} [g cm^{-3}]	1.493	1.269	1.399
μ [mm^{-1}]	3.625	2.836	2.810
$F(000)$	7224	3924	2204
$2\theta_{max}$ [°]	49.84	50.52	50.64
reflns	26040	37975	26382
independent reflns	8788 [R_{int} = 0.070]	12096 [R_{int} = 0.056]	13222 [R_{int} = 0.068]
variables	460	489	623
GOF on F^2	0.81	0.89	0.90
R_1[a]	0.049	0.059	0.056
wR_2[b]	0.108	0.171	0.130
residual ρ [e Å^{-3}]	+1.158, −0.771	+0.947, −1.299	+1.124, −1.045

[a] $R_1 = \Sigma||F_o| - |F_c||/\Sigma|F_o|$. [b] $wR_2 = \{\Sigma[w(F_o^2 - F_c^2)]/\Sigma[w(F_o^2)^2]\}^{1/2}$.

the second layer is the central C_6H_4 ring of *ortho*-PE(5) for **5** and the central C_6H_4–C≡C–C_6H_4 moiety of *ortho*-PE(6) for **6**. All the interlayer separations (≈3.3 Å for **5**, ≈3.4 Å for **6**) are typical distances for π–π interactions. There are two antiparallel folding axes for the *ortho*-PE(5) moiety in **5** and *ortho*-PE(6) moiety in **6**. Thus, the view along the folding axis of the helical structure in **5** and **6** could be described as a twisted "figure eight", and the folding direction for each loop of the figure eight is opposite to each other. No inter- or intramolecular Pt···Pt interactions are found in the crystal structures of both **5** and **6**. In **5**, intermolecular separations between the neighboring [(*t*Bu_3tpy)Pt] planes are close enough for π–π interactions (3.50 Å), whereas for **6**, the [(*t*Bu_3tpy)Pt] planes between the neighboring cations have a dihedral angle of 24.0°.

Spectroscopic properties: The photophysical properties of **1–9** are summarized in Table 2. The electronic absorption spectra of **1–7** show an intense band at 312–365 nm ($\varepsilon \approx 4\times10^4$ dm^3 mol^{-1} cm^{-1}) with vibronic structures and a less intense broad absorption band at 452–

Table 2. Photophysical data of **1**–**9**.

Complex	Medium	λ_{abs} [nm] (ε_{max} [10^3 M^{-1}cm^{-1}])	λ_{em} [nm] (τ_{em} [μs]) {φ_{em}}[a]
1	CH_2Cl_2 (298 K)	314 (45.0), 329 (36.2), 345 (34.3), 482 (11.6)	607 (0.4) {0.010}
	CH_3CN (298 K)	311 (35.0), 326 (30.9), 340 (30.4), 447 (sh, 8.8)	604 (0.2) {0.003}
	CH_3OH (298 K)	311 (33.1), 327 (29.2), 342 (29.7), 455 (sh, 8.4)	606 (0.1) {0.003}
	solid (298 K)[b]		647 (<0.1)
	solid (77 K)[b]		670 (1.1)
	glass (77 K)[c]		550 (17.3), 582 (sh)
2	CH_2Cl_2 (298 K)	312 (38.5), 325 (34.9), 341 (28.3), 453 (12.0)	650 (0.1) {0.005}
	solid (298 K)[d]		644 (<0.1)
	solid (77 K)[d]		664 (0.9)
	glass (77 K)[c]		545 (10.1), 623
3	CH_2Cl_2 (298 K)	313 (45.2), 325 (38.3), 339 (31.0), 473 (9.0)	591 (0.9) {0.004}
	solid (298 K)[b]		641 (0.2)
	solid (77 K)[b]		638 (3.6)
	glass (77 K)[c]		532, 611 (16.7)
4	CH_2Cl_2 (298 K)	314 (46.5), 325 (43.2), 340 (38.6), 362 (19.8), 452 (8.8)	605 (0.5) {0.006}
	solid (298 K)[b]		705 (0.3)
	solid (77 K)[b]		706 (0.8)
	glass (77 K)[c]		519 (25.1), 554
5	CH_2Cl_2 (298 K)	314 (47.7), 325 (42.9), 340 (35.7), 365 (17.9), 467 (sh, 7.8)	584 (0.6) {0.059}
	CH_3CN (298 K)	313 (45.8), 326 (45.3), 339 (41.6), 364 (25.1), 434 (sh, 9.4)	567 (0.2) {0.004}
	CH_3OH (298 K)	314 (36.8), 326 (36.4), 340 (33.2), 366 (19.5), 435 (sh, 7.1)	563 (0.1) {0.002}
	solid (298 K)[d]		663 (0.3)
	solid (77 K)[d]		547 (2.7), 592 (3.3), 707 (0.9)
	glass (77 K)[c]		523 (127.0), 564, 593
6	CH_2Cl_2 (298 K)	314 (47.9), 325 (44.9), 340 (40.5), 364 (22.5), 461 (sh, 8.3)	600 (2.3) {0.041}
	solid (298 K)[b]		659 (<0.1)
	solid (77 K)[b]		588 (4.9), 640 (sh, 1.9), 695 (1.2)
	glass (77 K)[c]		529 (21.6), 564, 595 (sh)
7	CH_2Cl_2 (298 K)	316 (73.6), 325 (70.6), 339 (64.9), 364 (41.2), 457 (sh, 9.9)	604 (0.6) {0.024}
	solid (298 K)[d]		662 (0.2)
	solid (77 K)[d]		586 (2.0), 705 (1.0)
	glass (77 K)[c]		526 (78.0), 561
8	CH_2Cl_2 (298 K)	315 (14.7), 340 (12.6), 413 (sh, 4.1)	593 (3.4) {0.111}
	solid (298 K)[b]		644 (<0.1)
	solid (77 K)[b]		643 (1.2)
	glass (77 K)[c]		518 (10.0), 547 (sh), 605 (sh)
9	CH_2Cl_2 (298 K)	314 (28.3), 461 (sh, 4.1)	580 (0.6) {0.087}
	solid (298 K)[b]		675 (0.2)
	solid (77 K)[b]		567 (sh), 672, 700 (1.0)
	glass (77 K)[c]		516 (23.9), 551 (sh, 17.0)

[a] Quantum yield for degassed solutions, using quinine sulfate in 0.1 M H_2SO_4 ($\varphi_{em}=0.546$) as reference. [b] Microcrystalline solid. [c] CH_3OH/CH_3CH_2OH (v/v) = 1:4 at 77 K. [d] Fine powder.

482 nm ($\varepsilon \approx 0.75$–1.25×10^4 dm^{3}mol^{-1}cm^{-1}) in CH_2Cl_2 at room temperature (Figure 2). When the bridging *ortho*-PE is extended from one to eight (C≡C−1,2-C_6H_4) repeating units as in the case of **1**–**7**, there is only a slight variation of the low-energy absorption band maximum with no distinct trend observed. For comparison, the spectroscopic data of the two mononuclear complexes **8** and **9** containing the C≡CC_6H_5 and (C≡C−1,2-C_6H_4)$_2$–C≡CC_6H_5 ligand, respectively, were studied. The absorption spectra of **8** and **9** (a high-energy band at 314–340 nm and a low-energy band at 413–461 nm) resemble that of the binuclear complexes **1**–**7**. The solvent effect on the absorption spectrum of **5** has been examined: the low-energy absorption band maximum blue-shifts from 467 nm to ≈434 nm when the solvent changes from CH_2Cl_2 to CH_3CN and CH_3OH (Figure 3). Similar hypsochromism on the absorption spectrum of **1** has also been observed (from 482 nm in CH_2Cl_2 to ≈450 nm in CH_3CN and CH_3OH). The low-energy absorption band of **5**

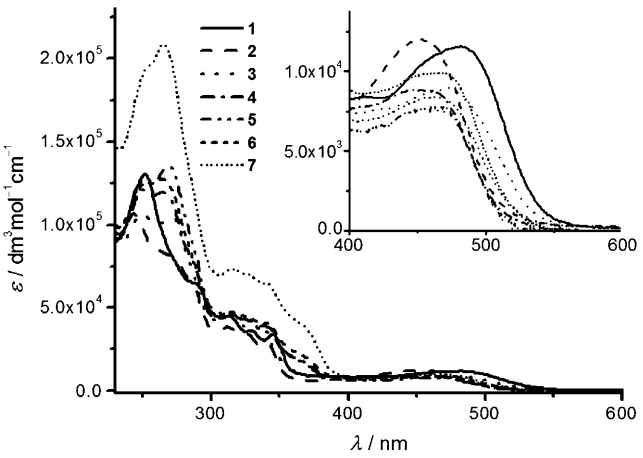

Figure 2. UV/Vis absorption spectra of **1**–**7** in CH_2Cl_2 at 298 K with the inset showing the amplified 400–600 nm region.

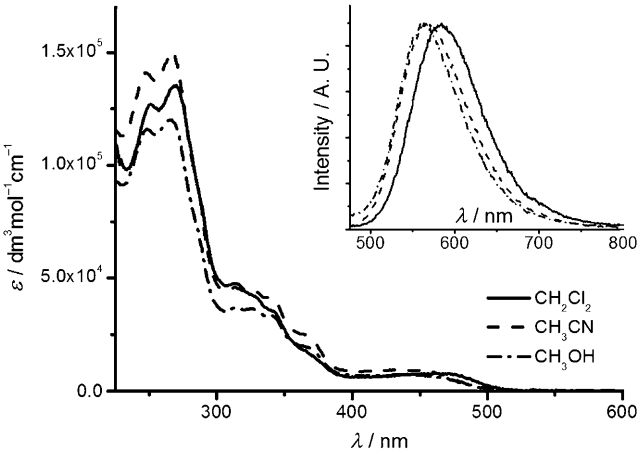

Figure 3. UV/Vis absorption and normalized emission (inset) spectra of **5** in CH_2Cl_2, CH_3CN, and CH_3OH ($\lambda_{ex}=350$ nm) at 298 K.

obeys Beer's law in the concentration range of 10^{-5}–10^{-4} mol dm^{-3} in CH_3CN, suggesting no significant aggregation in this concentration range.

All these complexes are emissive in degassed solutions, in solid state and in CH_3OH/CH_3CH_2OH (v/v = 1:4) glassy solutions at 77 K. Emission lifetimes are in the microsecond time region, and the emission quantum yields measured in CH_2Cl_2 are in the range of 0.2–5.9% (the results are listed in Table 2). The room-temperature emission λ_{max} for **1**–**7** in CH_2Cl_2 are 607, 650, 591, 605, 584, 600 and 604 nm, respectively; while their corresponding solid-state emission maxima are red-shifted (except for **2**) to 647, 644, 641, 705, 663, 659 and 662 nm, respectively. For the mononuclear complexes **8** and **9**, their solid-state emissions are at lower energies (644 nm for **8**, 675 nm for **9**) than in CH_2Cl_2 (593 nm for **8**, 580 nm for **9**). Complex **5** was chosen to illustrate the solvatochromic properties of this class of complexes. Upon changing the solvent from CH_2Cl_2 to CH_3CN and CH_3OH, its emission λ_{max} (lifetime, quantum yield) is blue-shifted from 584 (0.6 μs, 0.06) to 567 (0.2 μs, <0.01) and 563 nm (0.1 μs, <0.01) (Figure 3). Increasing the counterion concentration from 0.001 M to 0.01 M by adding a $LiClO_4$ salt to a solution of **5** in CH_3OH at $\approx 1.0\times 10^{-5}$ mol dm^{-3} did not change its electronic absorption and emission spectra.

Water-induced emission change: The emission properties of **1**–**7** in aerated H_2O/CH_3CN mixtures with increasing H_2O composition have been examined. The concentrations of the platinum(II) complexes were fixed at 1.0×10^{-5} mol dm^{-3}, and all the absorption and emission spectra were measured under aerated conditions. The solutions or dispersions used for the spectroscopic measurements remained transparent for at least 30 days, even when the water fraction was as high as 90%. A red-shift in emission energy and enhancement of the emission intensity were found for **3**–**7** in aerated H_2O/CH_3CN mixtures with a water composition of >40% (v/v). Upon increasing the water fraction from 40 to 90%, the emission maximum red-shifted from 583 to 699 nm (2846 cm^{-1}) for **3**, 598 to 657 nm (1502 cm^{-1}) for **4**, 567 to 670 nm for (2711 cm^{-1}) **5**, 584 to 657 nm (1903 cm^{-1}) for **6**, and 584 to 659 nm (1949 cm^{-1}) for **7**; the corresponding quantum yield increased by 3.6, 22.7, 8.4, 16.4 and 3.0-fold for **3**–**7**, respectively. The emission lifetimes showed slight increments (from 0.1 to 0.6 μs). Most notably, the red-shifted emission λ_{max} upon addition of water is comparable in energy to the corresponding room-temperature solid-state emission ($\lambda_{max}=641$, 705, 663, 659 and 662 nm for **3**–**7**, respectively). Under the same conditions, **1** and **2**, which have shorter *ortho*-PE(n) ($n<3$) ligands, showed red-shifted λ_{max} (611 to 633 nm (569 cm^{-1}) for **1**, 645 to 721 nm (1634 cm^{-1}) for **2**), but less than a 0.2-fold enhancement in the emission intensity was observed.

The mononuclear complexes **8** with a $C{\equiv}CC_6H_5$ moiety and **9** with a $(C{\equiv}C{-}1,2\text{-}C_6H_4)_2{-}C{\equiv}CC_6H_5$ moiety in aerated H_2O/CH_3CN mixtures were studied for comparison. For **9**, the emission λ_{max} red-shifts from 571 to 655 nm (2246 cm^{-1}) with a concomitant 19-fold enhancement in intensity when the water percentage increases from 40 to 90%. In contrast, **8** has no angular *ortho*-PE ligand, and its emission in aerated H_2O/CH_3CN mixtures diminishes in intensity without a red-shift in λ_{max} upon increasing the water fraction from 0 to 0.9 (see Supporting Information).

Complex **5** was chosen for further investigation. Upon increasing the water content from 40 to 90%, the emission λ_{max} of **5** in aerated H_2O/CH_3CN mixtures red-shifted from 567 to 670 nm (2711 cm^{-1}) (the emission spectra are depicted in Figure 4, top); the emission quantum yield increased from <0.01 to 0.03, and the lifetime increased from 0.1 to 0.4 μs. The UV/Vis absorption spectra of **5** in aerated H_2O/CH_3CN mixtures (Figure 4, middle) with increased water percentage showed a sharp decrease in absorbance at $\lambda=350$ nm, together with a concomitant increase in the low-energy absorption band at ≈ 500 nm. This is consistent with the finding of an absorption peak maximum at 475 nm in the excitation spectrum recorded with a solution of **5** in a 90:10 H_2O/CH_3CN mixture (monitored at emission wavelength 674 nm) (Figure 4, bottom). The former is red-shifted from the corresponding peak maximum at 458 nm when the excitation spectrum was recorded in a 40:60 H_2O/CH_3CN mixture (monitored at emission wavelength 568 nm; Figure 4, bottom). The spectroscopic properties of **5** in aerated Et_2O/CH_3CN mixtures were studied. A solution of **5** in an Et_2O/CH_3CN mixture containing 90% Et_2O is not as stable as in H_2O/CH_3CN mixtures. In the former, **5** precipitated as a microcrystalline solid after standing for ≈ 24 h. In contrast to the finding obtained with the H_2O/CH_3CN mixtures, upon gradually increasing the Et_2O fraction from 40 to 90%, only slight changes in the UV/Vis absorption spectra could be found, and the emission λ_{max} remained at ≈ 570 nm with a fourfold enhancement in intensity (Figure 5).

As **5** is insoluble in water but a solution (or dispersion) of **5** in H_2O/CH_3CN mixtures (volume ratio varying from 40:60 to 90:10) at a concentration of 1.0×10^{-5} mol dm^{-3} remained

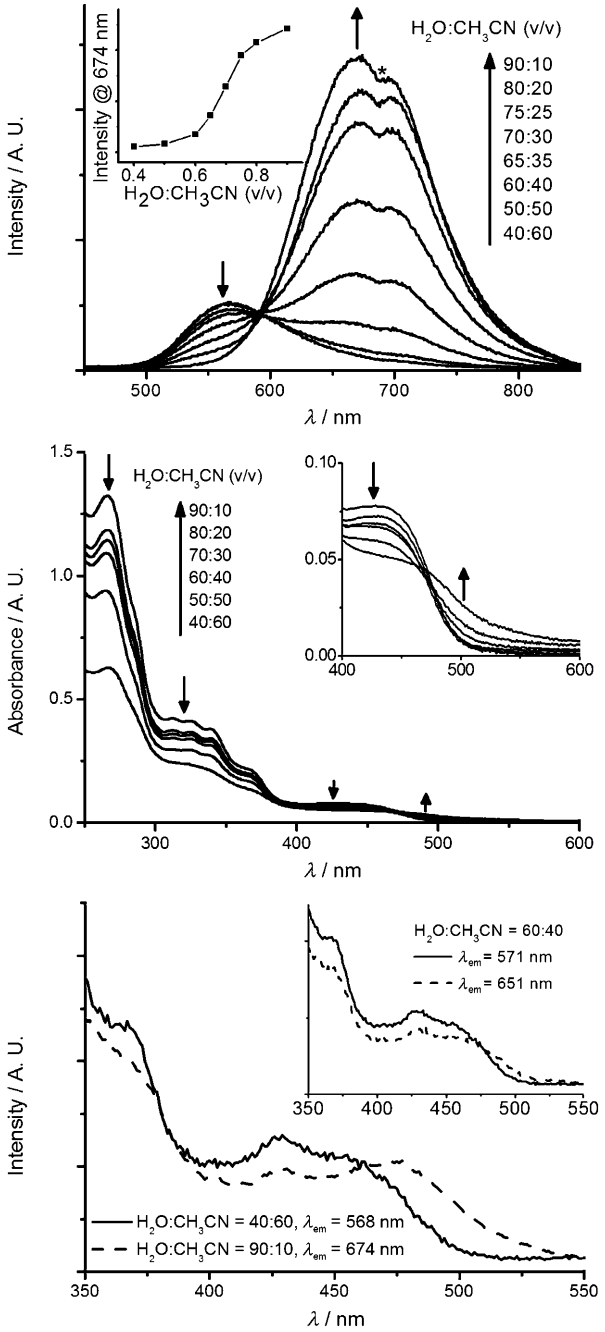

Figure 4. Spectroscopic traces for **5** in aerated H_2O/CH_3CN mixtures upon increasing the water fraction. Top: Emission traces ($\lambda_{ex}=350$ nm) with the inset showing the plot of emission intensity at 674 nm against water fraction. Middle: UV/Vis absorption traces with the inset showing the enlarged 400–600 nm region. Bottom: Excitation spectra monitored at $\lambda_{em}=568$ (40% H_2O) and 674 nm (90% H_2O), respectively, with inset showing the excitation spectra in 60% H_2O/CH_3CN mixture monitored at $\lambda_{em}=571$ and 651 nm, respectively.

transparent, we envisage that **5** may exist as nanosized spherical aggregates in these solution mixtures. Representative transmission electron micrograph (TEM) of the aggregates formed by **5** in a 9:1 H_2O/CH_3CN mixture is depicted in Figure 6 (top). Dynamic light scattering (DLS) measurements showed that the average diameter of these spherical aggregates was ≈33 nm (Figure 6, bottom). However, no nanosized particles were observed by either DLS or TEM studies in Et_2O/CH_3CN mixtures with volume ratio of 90:10.

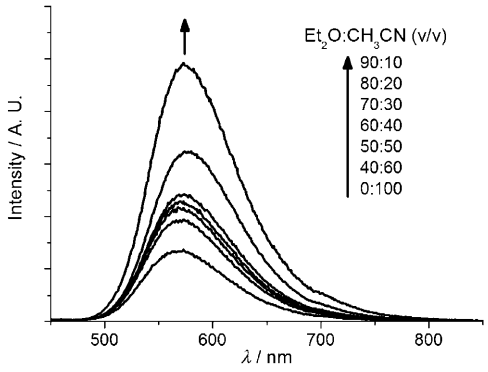

Figure 5. Emission traces ($\lambda_{ex}=350$ nm) of complex **5** in Et_2O/CH_3CN mixtures upon increasing the Et_2O fraction.

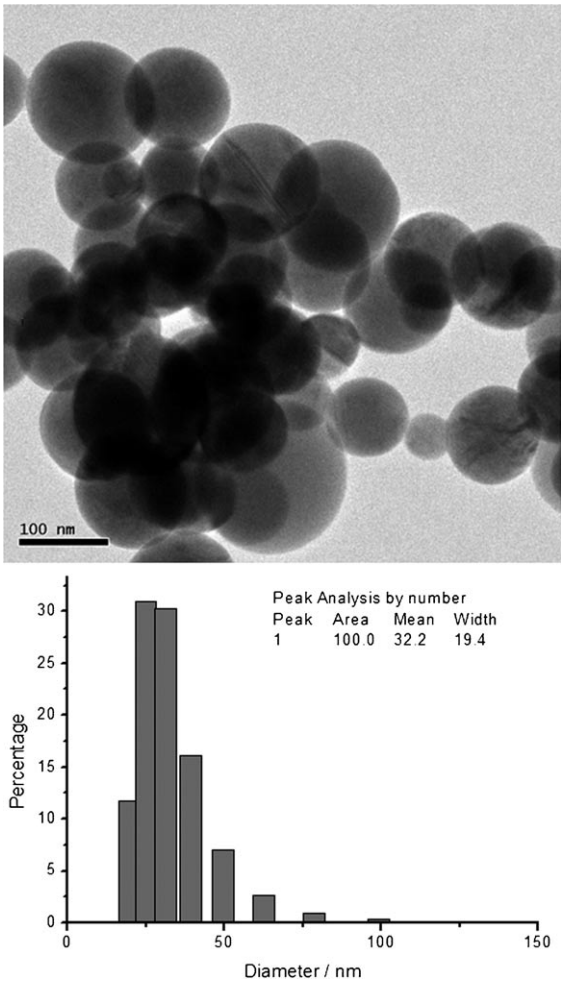

Figure 6. Top: TEM image of **5** in H_2O/CH_3CN with a water fraction of 90%. Bottom: Histogram of particle size distribution of **5** in H_2O/CH_3CN mixtures at 90% water fraction as determined by dynamic light scattering.

Similar submicron spherical structures were also found in a 9:1 H_2O/CH_3CN mixture of **6**.

Variable-temperature NMR spectroscopy: In the literature, 1D and 2D (NOESY or ROESY) NMR have been utilized to study the folding behavior of the *ortho*-PE(*n*) backbone in polar solvents.[9f–h] In this work, a significant change in the emission property of **5** was found in the aerated H_2O/CH_3CN mixtures with a high water percentage. However, under these conditions, the solubility of **5** is too low to allow for a 2D (NOESY or ROESY) NMR study. An attempt to replace the counterion of **5** from perchlorate to chloride by using an anion-exchange resin (aiming to increase their water solubility) was not successful. Instead, a variable-temperature ^{1}H NMR experiment was conducted, and a ^{1}H–^{1}H COSY NMR measurement was also performed to assist in the assignment of proton signals (see Supporting Information for spectra). Again **5** was chosen for the study as its ^{1}H NMR signals are well-resolved. Figure 7 displays the NMR spectra of **5** in CD_2Cl_2 with a concentration of $\approx 5\times 10^{-3}$ M at −60, −50, −40, −20, 0 and 20 °C. When the temperature decreases from 20 to −60 °C, the NMR signals of the terpyridyl protons H1 and H4 in the aromatic region are shifted upfield; the chemical shifts of the terpyridyl H2 and H3 remain unchanged, while the signals of two protons on the central phenyl ring (marked as ▲) and other phenyl protons (except two protons) are shifted downfield. The NMR signals of the terpyridyl protons H1, H2, H3 and H4 are broadened upon decreasing temperature from 20 to −60 °C, while the breadth of the other signal peaks remained almost unchanged.

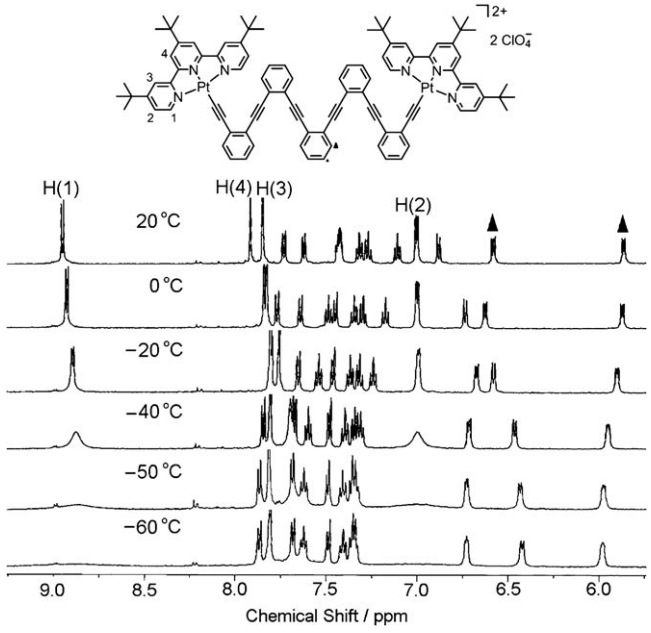

Figure 7. Variable-temperature ^{1}H NMR spectra of **5** in CD_2Cl_2 solution ($\approx 5\times 10^{-3}$ M) at −60, −50, −40, −20, 0 and 20 °C.

Discussion

Folded *ortho*-PE(*n*) moieties in crystal structures: Based on the crystal structures of *ortho*-PEs or compounds containing *ortho*-PE(*n*) bridges reported in literature, the *ortho*-PE bridges can be summarized to adopt the following conformations: I) *transoid–transoid*, II) *transoid–cisoid*, and III) *cisoid–cisoid* (Figure 8). Grubbs and Kratz reported the

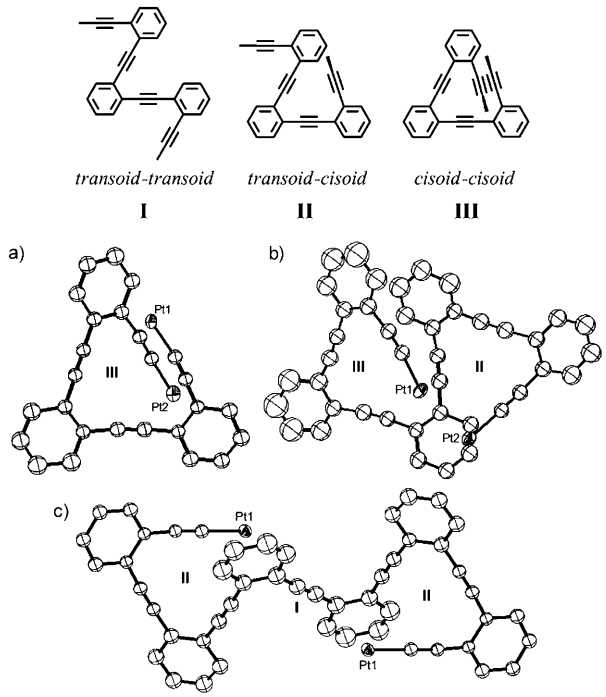

Figure 8. Partially folded conformations, I) *transoid–transoid*, II) *transoid–cisoid*, III) *cisoid–cisoid*, of the *ortho*-PE(*n*) moieties revealed by the crystal structures of a) **3**·2.5 CH_3OH, b) **5**·CH_3CN, and c) **6**·4 CH_3CN.

crystal structure of [*ortho*-PE(2)]Ph_2 (Ph = phenyl) and [*ortho*-PE(3)]Ph_2, revealing a *transoid–transoid* and *transoid–cisoid* helix, respectively.[8a] Youngs and co-workers reported that [*ortho*-PE(4)]H_2 and [*ortho*-PE(4)](TMS)$_2$ (TMS = trimethylsilane) adopt the *transoid–transoid* and *transoid–cisoid* conformation, respectively, in the crystal structures.[11] Substituted *ortho*-PE(2) and *ortho*-PE(3) with pyridyl caps were reported by Bunz and co-workers to adopt the *transoid–transoid* conformation in their crystal structures.[9e] Two triethylphosphine–platinum complexes containing a substituted *ortho*-PE(3) ligand and reported by Haley and co-workers were regarded as a twisted *transoid-transoid* conformation.[10e] In this work, the crystal structures of **3**, **5**, and **6** revealed that each of the coordinated *ortho*-PE(*n*) ligands of these complexes adopts a helical conformation. As depicted in Figure 8, **3** has a fully folded bridging *ortho*-PE(3) ligand with *cisoid–cisoid* conformation; the folding of *ortho*-PE(5) in **5** is considered to give rise to both *transoid–cisoid* and *cisoid–cisoid* conformations; and the folding of *ortho*-PE(6) in **6** has *transoid–transoid* and *trans-*

oid–cisoid conformations. The biaxially helical conformations of the *ortho*-PE(n) moieties in **5** and **6** are in contrast to the uniaxially helical structures reported for *meta*-PE(n) compounds.[12] The coordinated *ortho*-PE(n) ligands of the dicationic platinum(II) complexes described in this work are partially folded in their crystal structures, because π–π interactions could occur between the phenyleneethynylene moieties of the *ortho*-PE(n) ligands and the capping terpyridyl–platinum(II) moieties, all of which have a large π surface.

Spectroscopic properties of complexes 1–9: The UV/Vis absorption spectra of **1–9** are similar to mononuclear [Pt(tpy)-(C≡CC$_6$H$_5$)]PF$_6$ and other terpyridyl–platinum(II) complexes reported in the literature.[4] The corresponding free *ortho*-PE ligands of **1–9** absorb strongly at 272–329 nm in CH_2Cl_2 (see Supporting Information). With reference to previous work, we assign the high-energy absorption band of **1–9** at 313–365 nm to intra-ligand (IL) π→π*(*t*Bu$_3$tpy) and π→π*[(C≡C−1,2-C$_6$H$_4$)$_n$C≡C] transitions of the *ortho*-PE bridge and the terpyridyl ligand, and the low-energy band at 413–473 nm to a dπ(Pt)→π*(*t*Bu$_3$tpy) metal-to-ligand charge transfer (MLCT) transition.[3c,4]

In solution, the emission λ_{max}, lifetimes, and quantum yields of **1–9** are close to those of the reported terpyridyl–platinum(II) complexes.[4] The emission λ_{max} blue-shifts when the solvent polarity increases, indicating the ground state is more polar than the excited states. This is consistent with the MLCT assignment. With reference to previous work, a ^{3}[dπ(Pt)→π*(*t*Bu$_3$tpy)] excited state mixed with ^{3}[π→π*(*ortho*-PE)] is tentatively assigned to the emissions of **1–9** recorded in anhydrous, organic solvents.[3c,4]

It is known that square-planar oligopyridyl–Pt^{II} complexes usually absorb and emit at longer wavelengths in the solid state and in solutions with high complex concentrations than in diluted solutions. This is attributed to excimer/exciplex formation through π–π interactions in the ground and/or excited states.[5] For example, the crystalline form of [Pt-(tpy)Cl][CF$_3$SO$_3$] is orange-red, while a solution of this complex in CH_3CN is light yellow.[5c] A high concentration ($>10^{-3}$ mol dm^{-3}) of [Pt(tpy)Cl]PF$_6$ in EMD (ethanol/methanol/DMF 5:5:1) at low temperatures displays red-shifted MLCT and π–π excimer emission when compared with the emission recorded with a diluted solution.[5a] The *ortho*-PE(1) moiety in complex **1** is not long enough to be folded into a helical conformation, thus the emission red-shift of **1** from λ_{max} 604 nm in CH_3CN to 647 nm in the solid state at 298 K could only be explained by intermolecular π–π interactions and/or Pt···Pt interactions. In the cases of **3–7** with the *ortho*-PE(n) ($n \geq 3$) moieties, they fold into a compact structure as revealed by their X-ray crystal structures. Besides intermolecular π–π interactions and/or Pt···Pt interactions, the intramolecular π–π interactions between the phenyl rings of the bridging *ortho*-PEs and the terminal terpyridyl planes can be a prominent cause to the red-shift.

Red-shifted and enhanced emission of complexes 3–7 and 9 in aerated H_2O/CH_3CN mixtures: In H_2O/CH_3CN mixtures with increasing water percentage from 40 to 90%, a red-shift of emission energy and enhancement in emission intensity were observed for **3–7**, and **9**, the latter is a mononuclear Pt^{II} complex with the (C≡C−1,2-C$_6$H$_4$)$_2$−C≡CC$_6$H$_5$ ligand. The emission energy of **3—7** and **9** in 9:1 H_2O/CH_3CN mixtures are close to those recorded in solid state. This may suggest the conformation of these complexes in H_2O/CH_3CN mixtures with high H_2O percentages could resemble the folded structures of the corresponding metal complexes in the solid state. The red-shifts observed in the UV/Vis absorption traces of these complexes in H_2O/CH_3CN mixtures are in line with the aggregation and possible folding process upon increasing water contents. As depicted in Figure 4 (middle), the decrease in the absorbance of a high-energy band of **5** (350 nm, assigned as IL π→π* transitions) can be caused by an overlap of the p_π orbitals of the *ortho*-PE(5) moiety when the solvent polarity was increased (hypochromicity),[8a] while the red-shift and increase in the low-energy absorption (≈500 nm, assigned as dπ(Pt)→π*(*t*Bu$_3$tpy) MLCT transitions) can be attributed to Pt···Pt interactions and/or π–π interactions in solution. The excitation peak maximum of **5** in a 90% H_2O/CH_3CN mixture (monitored at λ_{em} = 674 nm) red-shifted from that in 40% H_2O/CH_3CN mixture (monitored at λ_{em} = 568 nm), revealing that ground-state molecular interactions occurred in the H_2O/CH_3CN solvent mixtures with high water percentages (Figure 4, bottom). Nanoscale particles with an average diameter of ≈33 nm were found for **5** in a 9:1 H_2O/CH_3CN mixture at a concentration of 1.0×10^{-5} mol dm^{-3}.

In a dispersion of **5** in 9:1 Et_2O/CH_3CN mixture, although nanosized particles were not detected in the TEM and DLS observations, molecular aggregation is thought to occur because Et_2O is a poor solvent for **5**, and crystalline precipitates were found after the mixture had stood for ≈24 h. There was an enhancement in the emission intensity, but no shift in the emission λ_{max} upon increasing the Et_2O content from 40 to 90%, and the UV/Vis absorption spectra remained almost unchanged. We suggest that, for **5** in Et_2O/CH_3CN mixtures, aggregation leads to a diminished nonradiative decay of the emissive excited state as a consequence of restricted motion of the molecules in the aggregates and that this is the main reason for the enhanced emission intensity. The intermolecular interactions resulting from aggregation may not significantly affect the emission energy. Similar aggregation induced emissions have been observed in the literature.[13]

Considering the different polarity of H_2O and Et_2O, we suggest that, in H_2O/CH_3CN solutions of **5**, hydrophobic folding is induced upon the addition of water. Intramolecular interactions between the [Pt(*t*Bu$_3$tpy)] planes and the bridging *ortho*-PE(n) ligands account for the red-shifted phosphorescence. This suggestion is further supported by two experimental findings: 1) the emission energy (λ_{em} = 674 nm) of **5** in the 9:1 H_2O/CH_3CN mixture resembles the one (λ_{em} = 663 nm) recorded in the crystalline solid state at 298 K, and the crystal structure of **5** revealed a partially folded conformation of the *ortho*-PE(5) moiety; and 2) com-

plexes **3**–**7** and **9**, which contain foldable *ortho*-PE(n) ($n \geq 3$) moieties were found to exhibit red-shifted and enhanced emissions in aerated H_2O/CH_3CN mixtures upon increasing the water percentages, whereas these red-shifted and enhanced emissions were not observed for complexes **1**, **2** and **8**, which contain only shorter *ortho*-PE(n)s ($n < 3$) moieties.

The results of a variable-temperature ^1H NMR study of **5** indicated that this complex may adopt an unfolded conformation in CD_2Cl_2 at 298 K, but intermolecular π–π interactions are possible at lower temperatures in this solvent system. It has been reported that ^1H signals are broadened and shifted upfield as a result of π–π stacking interactions due to self-association or aggregation of planar metal complexes containing aryl π-conjugated organic ligands.[5f,14] In this work, the terpyridyl protons' signals show broadening and an upfield shift, presumably due to the intermolecular π–π interactions of the terminal terpyridyl planes upon decrease in temperature. However, the signals of the protons on the central phenyl ring (marked as ▲) are shifted downfield and do not show peak broadening (Figure 7). 2D NOESY signals, corresponding to interactions between terpyridyl protons and two protons on the central phenyl ring, as would be expected for helical conformation, were not observed in the variable-temperature ^1H NMR spectra in solution. All these results exclude the possibility of **5** adopting a folded helical conformation in CD_2Cl_2 upon decreasing temperature from 20 to −60 °C. This is consistent with the spectroscopic studies on **5**, in which the emission energies (λ_{em} = 584 nm for CH_2Cl_2 solution at 298 K and λ_{em} = 523 nm for a glassy solution at 77 K) suggest a different conformation in solution from the folded structure in the crystal form (λ_{em} = 674 nm) of **5**.

Conclusion

In conclusion, we prepared novel dicationic terpyridyl–platinum(II) complexes containing flexible *ortho*-PE(n) ligands (PE = phenyleneethynylene), determined the helical conformations of the *ortho*-PE(n) moieties in the crystal structures, and demonstrated the uniquely red-shifted and enhanced phosphorescence of these complexes in aerated H_2O/CH_3CN solvent mixtures upon increasing the water percentages. Intermolecular aggregation and intramolecular hydrophobic folding of the coordinated *ortho*-PE(n) ($n = 3$) ligands are suggested as the main causes for these solvatochromic properties. These findings could benefit the molecular design of foldamers containing *ortho*-PE(n) moieties and phosphorescent platinum(II) complexes with flexible structures and tunable emission properties.

Experimental Section

General procedures: All starting materials were purchased from commercial sources and used as received unless stated otherwise. The solvents used for synthesis were of analytical grade. The *ortho*-PEs, (H−(C≡C−1,2-C_6H_4)$_{n-1}$−C≡CH, n = 1, 2, 3, 4, 5, 6 and 8, respectively), and H(C≡C−1,2-C_6H_4)$_2$C≡CC_6H_5 were prepared according to literature methods.[8a,12,15] ^1H and ^{13}C NMR spectra were recorded on a Bruker Avance 400 or DRX 300 FT-NMR spectrometer with TMS (^1H and ^{13}C) as reference. Mass spectra (FAB) were obtained on a Finnigan MAT 95 mass spectrometer. Elemental analyses were performed by the Institute of Chemistry, Chinese Academy of Sciences, Beijing. UV/Vis spectra were recorded on a Perkin–Elmer Lambda 19 UV/Vis spectrophotometer. The degassed solution samples for emission measurements underwent at least four freeze-pump-thaw cycles. The aerated solution samples for emission measurements were exposed to air. Emission spectra were obtained on a SPEX Fluorolog-2 Model F111 fluorescence spectrophotometer. Emission lifetime measurements were performed with a Quanta Ray DCR-3 pulsed Nd:YAG laser system (pulse output 355 nm, 8 ns). Luminescent quantum yields were referenced to quinine sulfate in 0.1 M H_2SO_4 solution (φ_{em} = 0.546) with estimated error of ±15%. The samples for TEM observations were prepared by depositing a few drops of the aqueous samples on the holey copper grid, which was then put into a desiccator. The TEM images were recorded on a Philips Tecnai 20 electron microscope, with an accelerating voltage of 200 kV. The dynamic light scattering (DLS) experiments were performed with a Malvern ZetaSizer 3000HSA. IR measurements were performed by using a Bio-Rad FT-IR spectrometer.

Syntheses and characterization:

General procedure for the syntheses of complexes 1–9: Complexes **1–9** were synthesized by the overnight reaction of corresponding *ortho*-PEs (H−(C≡C−1,2-C_6H_4)$_n$−C≡CH, n = 1, 2, 3, 4, 5, 6, 8, respectively), HC≡CC_6H_5 or H−(C≡C−1,2-C_6H_4)$_2$C≡CC_6H_5 with [(tBu$_3$tpy)PtCl]ClO_4 (molar ratio 1:2 for **1–7**, 1:1 for **8** and **9**) in argon-bubbled CH_2Cl_2/iPr$_2$NH (volume ratio 4:1) solvent mixture with a catalytic amount of CuI at room temperature. Chromatography on neutral Al_2O_3 with CH_2Cl_2/acetone (volume ratio 4:1) to CH_2Cl_2/CH_3OH (volume ratio 4:1) as eluent gave **1–9** as orange or red solids.

[(tBu$_3$tpy)Pt−C≡C−1,2-C_6H_4−C≡C−Pt(tBu$_3$tpy)][ClO_4]$_2$ (1): Yield: 78%; ^1H NMR (300 MHz, CD_3CN, 25 °C): δ = 9.37 (d with Pt satellites, ^3J = 6.0 Hz, 4H; terpyridyl H), 8.31 (s, 4H; terpyridyl H), 8.15 (d, ^4J = 1.7 Hz, 4H; terpyridyl H), 7.74 (dd, ^3J = 6.0 Hz, 4H; terpyridyl H), 7.59 (m, 2H; phenyl H), 7.31 (m, 2H; phenyl H), 1.53 (s, 18H; *tert*-butyl H), 1.22 ppm (s, 36H; *tert*-butyl H); $^{13}C\{^1H\}$ NMR (100 MHz, CD_3CN, 25 °C): δ = 168.8, 167.5, 159.1 and 154.9 (quaternary C on terpyridyl), 156.1 (tertiary C on terpyridyl), 132.6, 130.4 and 127.4 (C on phenyl ring), 127.1, 124.1 and 122.5 (tertiary C on terpyridyl), 105.2 (Pt−*C*≡C), 103.4 (Pt−C≡*C*), 38.2 and 37.0 (quaternary C on *tert*-butyl group), 30.6 and 30.1 ppm (primary C on *tert*-butyl group); IR (KBr): $\tilde{\nu}$ = 2122 cm^{-1} (C≡C); FAB-MS (+ve): m/z: 1417 [$M-ClO_4$]$^+$, 1317 [$M-2ClO_4$]$^+$, 659 [$M-2ClO_4$]$^{2+}$; elemental analysis calcd (%) for $C_{64}H_{74}Cl_2N_6O_8Pt_2\cdot H_2O$: C 50.10, H 4.99, N 5.48; found: C 50.12, H 4.87, N 5.50.

[(tBu$_3$tpy)Pt−(C≡C−1,2-C_6H_4)$_2$−C≡C−Pt(tBu$_3$tpy)][ClO_4]$_2$ (2): Yield: 66%; ^1H NMR (300 MHz, CD_3CN, 25 °C): δ = 9.04 (d with Pt satellites, ^3J = 6.0 Hz, 4H; terpyridyl H), 7.94 (d, ^4J = 1.7 Hz, 4H; terpyridyl H), 7.92 (s, 4H; terpyridyl H), 7.71 (dd, ^4J = 1.7 Hz, 2H; phenyl H), 7.46–7.35 (m, 6H; phenyl H), 7.28 (dd, ^3J = 8.4 Hz, 4H; terpyridyl H), 1.44 (s, 18H; *tert*-butyl H), 1.39 ppm (s, 36H; *tert*-butyl H); $^{13}C\{^1H\}$ NMR (100 MHz, CD_3CN, 25 °C): δ = 168.9, 167.6, 158.6 and 154.8 (quaternary C on terpyridyl), 156.2 (tertiary C on terpyridyl), 133.8, 133.6, 129.7 and 127.8 (C on phenyl ring), 126.8 (tertiary C on terpyridyl), 126.5 (C on phenyl ring), 123.7 and 121.5 (tertiary C on terpyridyl), 106.8 (Pt−*C*≡C), 103.9 (Pt−C≡*C*), 93.4 (C≡C), 38.2 and 37.1 (quaternary C on *tert*-butyl group), 30.9 and 30.4 ppm (primary C on *tert*-butyl group); IR (KBr): $\tilde{\nu}$ = 2120 cm^{-1} (C≡C); FAB-MS (+ve): m/z: 1516 [$M-ClO_4$]$^+$, 1417 [$M-2ClO_4$]$^+$, 708 [$M-2ClO_4$]$^{2+}$; elemental analysis calcd (%) for $C_{72}H_{78}Cl_2N_6O_8Pt_2\cdot H_2O$: C 52.91, H 4.93, N 5.14; found: C 52.56, H 4.75, N 5.07.

[(tBu$_3$tpy)Pt−(C≡C−1,2-C_6H_4)$_3$−C≡C−Pt(tBu$_3$tpy)][ClO_4]$_2$ (3): Yield: 52%; ^1H NMR (300 MHz, CD_3CN, 25 °C): δ = 9.09 (d with Pt satellites, ^3J = 6.0 Hz, 4H; terpyridyl H), 8.23 (s, 4H; terpyridyl H), 8.15 (d, $^{1.7}J$ = 1.7 Hz, 4H; terpyridyl H), 7.35–7.27 (m, 4H; phenyl H), 7.22 (d, ^3J = 6.0 Hz, 4H; terpyridyl H), 6.60 (t, ^3J = 8.0 Hz, 4H; phenyl H), 6.43 (t, ^3J = 8.0 Hz, 2H; phenyl H), 6.18 (t, ^3J = 8.4 Hz, 2H; phenyl H), 1.58 (s,

18H; *tert*-butyl H), 1.36 ppm (s, 36H; *tert*-butyl H); $^{13}C\{^1H\}$ NMR (100 MHz, CD_3CN, 25°C): $\delta = 167.8$, 167.0, 159.3 and 154.9 (quaternary C on terpyridyl), 154.6 (tertiary C on terpyridyl), 134.4, 132.5, 131.5, 131.3, 129.6, 128.6 and 127.5 (C on phenyl ring), 126.1 (tertiary C on terpyridyl), 126.0 and 125.7 (C on phenyl ring), 123.9 and 122.2 (tertiary C on terpyridyl), 102.8 (Pt−C≡C), 95.2 (C≡C), 91.9 (C≡C), 38.1 and 37.0 (quaternary C on *tert*-butyl group), 30.7 and 30.3 ppm (primary C on *tert*-butyl group); IR (KBr)): $\tilde{\nu} = 2120\ cm^{-1}$ (C≡C); FAB-MS (+ve): *m/z*: 1516 $[M-2ClO_4]^+$, 759 $[M-2ClO_4]^{2+}$; elemental analysis calcd (%) for $C_{80}H_{82}Cl_2N_6O_8Pt_2 \cdot 2H_2O$: C 54.82, H 4.95, N 4.80; found: C 54.58, H 4.77, N 4.85.

[(*t*Bu$_3$tpy)Pt−(C≡C−1,2-C$_6$H$_4$)$_4$−C≡C−Pt(*t*Bu$_3$tpy)][ClO$_4$]$_2$ (4): Yield: 51%; ^1H NMR (300 MHz, CD_3CN, 25°C): $\delta = 8.88$ (d with Pt satellites, $^3J = 6.0$ Hz, 4H; terpyridyl H), 8.16 (s, 4H; terpyridyl H), 8.01 (d, $^4J = 1.7$ Hz, 4H; terpyridyl H), 7.37–7.28(m, 8H; phenyl H), 7.23 (td, $^3J = 8.4$ Hz, 2H; phenyl H), 7.08 (m, 2H; phenyl H), 7.00 (dd, $^3J = 6.0$, $^4J = 1.7$ Hz, 4H; terpyridyl H), 6.84 (m, 4H; phenyl H), 1.51 (s, 18H; *tert*-butyl H), 1.21 ppm (s, 36H; *tert*-butyl H); $^{13}C\{^1H\}$ NMR (100 MHz, CD_3CN, 25°C): $\delta = 168.1$, 167.1, 159.2 and 154.8 (quaternary C on terpyridyl), 154.7 (tertiary C on terpyridyl), 134.5, 132.9, 132.5, 130.3, 129.6, 129.2, 129.0,127.2 and 126.5 (C on phenyl ring), 126.2, 123.7 and 122.1 (tertiary C on terpyridyl), 106.2 (Pt−*C*≡C), 102.6 (Pt−C≡*C*), 94.7 (C≡C), 93.4 (C≡C), 91.4 (C≡C), 38.0 and 36.8 (quaternary C on *tert*-butyl group), 30.6 and 30.1 ppm (primary C on *tert*-butyl group); IR (KBr): $\tilde{\nu} = 2117\ cm^{-1}$ (C≡C); FAB-MS (+ve): *m/z*: 1716 $[M-ClO_4]^+$, 1617 $[M-2ClO_4]^+$, 808 $[M-2ClO_4]^{2+}$; elemental analysis calcd (%) for $C_{88}H_{86}Cl_2N_6O_8Pt_2 \cdot H_2O$: C 57.61, H 4.83, N 4.58; found: C 57.66, H 4.83, N 4.56.

[(*t*Bu$_3$tpy)Pt−(C≡C−1,2-C$_6$H$_4$)$_5$−C≡C−Pt(*t*Bu$_3$tpy)][ClO$_4$]$_2$ (5): Yield: 47%; ^1H NMR (400 MHz, CD_3CN, 25°C): $\delta = 8.80$ (d with Pt satellites, $^3J = 6.0$ Hz, 4H; terpyridyl H), 7.93 (d, $^4J = 1.7$ Hz, 4H; terpyridyl H), 7.88 (s, 4H; terpyridyl H), 7.73 (d, $^3J = 7.9$ Hz, 2H; phenyl H), 7.60 (dd, $^3J = 7.8$ Hz, 2H; phenyl H), 7.52 (td, $^3J = 8.0$ Hz, 2H; phenyl H), 7.42 (dd, $^3J = 8.0$ Hz, 2H; phenyl H), 7.38 (td, $^3J = 7.9$ Hz, 2H; phenyl H), 7.32 (td, $^3J = 8.0$ Hz, 2H; phenyl H), 7.26 (td, $^3J = 8.2$ Hz, 2H; phenyl H), 7.07 (dd, $^3J = 6.0$, $^4J = 1.7$ Hz, 4H; terpyridyl H), 6.62 (m, 2H; phenyl H), 6.51 (d, $^3J = 7.9$ Hz, 2H; phenyl H), 5.87 (m, 2H; phenyl H), 1.29 (s, 36H; *tert*-butyl H), 1.26 ppm (s, 18H; *tert*-butyl H); $^{13}C\{^1H\}$ NMR (100 MHz, CD_3CN, 25°C): $\delta = 168.1$, 166.7, 159.2 and 154.9 (quaternary C on terpyridyl), 154.5 (tertiary C on terpyridyl), 134.3, 134.2, 132.7, 132.2, 131.5, 130.7, 129.9, 129.8, 129.7, 127.5, 127.1, 126.9 and 126.6 (phenyl C), 126.1, 123.3 and 121.8 (tertiary C on terpyridyl), 106.8 (Pt−*C*≡C), 101.5 (Pt−C≡*C*), 95.4 (C≡C), 93.8 (C≡C), 92.5 (C≡C), 91.6 (C≡C), 37.8 and 36.8 (quaternary C on *tert*-butyl group), 30.4 and 30.3 ppm (primary C on *tert*-butyl group); IR (KBr): $\tilde{\nu} = 2119\ cm^{-1}$ (C≡C); FAB-MS (+ve): *m/z*: 1817 $[M-ClO_4]^+$, 1718 $[M-2ClO_4]^+$, 859 $[M\text{-}2ClO_4]^{2+}$; elemental analysis calcd (%) for $C_{96}H_{90}Cl_2N_6O_8Pt_2 \cdot CH_2Cl_2$: C 58.20, H 4.63, N 4.20; found: C 58.52, H 4.78, N 4.52.

[(*t*Bu$_3$tpy)Pt−(C≡C−1,2-C$_6$H$_4$)$_6$−C≡C−Pt(*t*Bu$_3$tpy)][ClO$_4$]$_2$ (6): Yield: 65%; ^1H NMR (400 MHz, CD_3CN, 25°C): $\delta = 8.80$ (d with Pt satellites, $^3J = 6.0$ Hz, 4H; terpyridyl H), 7.89 (s, 4H; terpyridyl H), 7.85 (d, $^4J = 1.7$ Hz, 4H; terpyridyl H), 7.73 (d, $^3J = 8.0$ Hz, 2H; phenyl H), 7.57 (dd, $^3J = 8.0$ Hz, 2H; phenyl H), 7.50 (td, $^3J = 7.9$ Hz, 2H; phenyl H), 7.45 (d, $^3J = 7.8$ Hz, 2H; phenyl H), 7.39–7.26 (m, 8H; phenyl H), 7.05 (td, $^3J = 8.0$ Hz, 2H; phenyl H), 7.00 (dd, $^3J = 6.0$, $^4J = 1.7$ Hz, 4H; terpyridyl H), 6.93 (d, $^3J = 8.2$ Hz, 2H; phenyl H), 6.52 (td, $^3J = 8.4$ Hz, 2H; phenyl H), 6.24 (d, $^3J = 8.2$ Hz, 2H; phenyl H), 1.28 (s, 18H; *tert*-butyl H), 1.27 ppm (s, 36H; *tert*-butyl H); $^{13}C\{^1H\}$ NMR (100 MHz, CD_3CN, 25°C): $\delta = 168.2$, 166.9, 159.1 and 155.1 (quaternary C on terpyridyl), 154.7 (tertiary C on terpyridyl), 135.4, 133.7, 132.8, 132.7, 132.0, 130.7, 130.5, 130.0, 129.8, 129.7, 129.1, 129.0, 127.3, 127.2, 127.1 126.6 and 126.2 (phenyl C), 126.1 (tertiary C on terpyridyl), 125.6 (phenyl C), 123.2 and 121.8 (tertiary C on terpyridyl), 106.5 (Pt−*C*≡C), 101.8 (Pt−C≡*C*), 95.5 (C≡C), 94.8 (C≡C), 93.7 (C≡C), 92.6 (C≡C), 91.5 (C≡C), 38.0 and 36.9 (quaternary C on *tert*-butyl group), 30.5 and 30.3 ppm (primary C on *tert*-butyl group); IR (KBr): $\tilde{\nu} = 2118\ cm^{-1}$ (C≡C); FAB-MS (+ve): *m/z*: 1818 $[M-2ClO_4]^+$, 909 $[M-2ClO_4]^{2+}$; elemental analysis calcd (%) for $C_{104}H_{94}Cl_2N_6O_8Pt_2 \cdot 0.5\,CH_2Cl_2$: C 60.95, H 4.65, N 4.08; found: C 60.80, H 4.70, N 4.12.

[(*t*Bu$_3$tpy)Pt−C≡C−1,2-C$_6$H$_4$)$_8$−C≡C−Pt(*t*Bu$_3$tpy)][ClO$_4$]$_2$ (7): Yield: 57%; ^1H NMR (300 MHz, CD_3CN, 25°C): $\delta = 8.68$ (d with Pt satellites, $^3J = 6.0$ Hz, 4H; terpyridyl H), 7.88 (s, 4H; terpyridyl H), 7.85 (d, $^4J = 1.7$ Hz, 4H; terpyridyl H), 7.54 (d, $^3J = 8.2$ Hz, 2H; phenyl H), 7.47 (d, $^3J = 8.1$ Hz, 2H; phenyl H), 7.37–7.28 (m, 8H; phenyl H), 7.24–7.09 (m, 12H; phenyl H), 6.96 (m, 2H; phenyl H), 6.91 (dd, $^3J = 6.0$ Hz, 4H; terpyridyl H), 6.64 (td, $^3J = 8.0$ Hz, 2H; phenyl H), 6.53 (d, 2H; phenyl H), 6.35 (td, $^3J = 8.1$ Hz, 2H; phenyl H), 1.27 (s, 18H; *tert*-butyl H), 1.20 ppm (s, 36H; *tert*-butyl H); $^{13}C\{^1H\}$ NMR (100 MHz, CD_3CN, 25°C): $\delta = 167.8$, 166.6, 159.0 and 154.8 (quaternary C on terpyridyl), 154.5 (tertiary C on terpyridyl), 134.7, 133.5, 133.1, 132.9, 132.7, 132.5, 132.1, 131.7, 130.5, 129.7, 129.6, 128.6, 128.4, 127.0, 126.7, 126.4, 126.3 and 126.2 (phenyl C), 125.9 (tertiary C on terpyridyl), 125.8 and 125.4 (phenyl C), 123.3 and 121.7 (tertiary C on terpyridyl), 106.6 (Pt−*C*≡C), 101.8 (Pt−C≡*C*), 95.0 (C≡C), 94.0 (C≡C), 93.2 (C≡C), 93.0 (C≡C), 92.2 (C≡C), 91.6 (C≡C), 37.8 and 36.7 (quaternary C on *tert*-butyl group), 30.5 and 30.1 ppm (primary C on *tert*-butyl group); IR (KBr): $\tilde{\nu} = 2119\ cm^{-1}$ (C≡C); FAB-MS (+ve): *m/z*: 2116 $[M-ClO_4]^+$, 2016 $[M-2ClO_4]^+$, 1008 $[M-2ClO_4]^{2+}$; elemental analysis calcd (%) for $C_{120}H_{102}Cl_2N_6O_8Pt_2 \cdot 1.5\,CH_2Cl_2$: C 62.24, H 4.51, N 3.58; found: C 62.18, H 4.46, N 3.38.

[(*t*Bu$_3$tpy)Pt−C≡CC$_6$H$_5$]ClO$_4$ (8): Yield: 90%; ^1H NMR (400 MHz, CD_3CN, 25°C): $\delta = 8.88$ (d with Pt satellites, $^3J = 6.0$ Hz, 2H; terpyridyl H), 8.28 (s, 2H; terpyridyl H), 8.23 (d, $^4J = 1.8$ Hz, 2H; terpyridyl H), 7.68 (dd, $^3J = 6.0$, $^4J = 1.8$ Hz, 2H; terpyridyl H), 7.43 (m, 2H; phenyl H), 7.35 (t, $^3J = 8.4$ Hz, 2H; phenyl H), 7.28 (m, 1H; phenyl H), 1.52 (s, 9H; *tert*-butyl H), 1.43 ppm (s, 18H; *tert*-butyl H); $^{13}C\{^1H\}$ NMR (100 MHz, CD_3CN, 25°C): $\delta = 168.5$, 167.9, 159.8 and 155.1 (quaternary C on terpyridyl), 154.7 (tertiary C on terpyridyl), 132.7, 129.3, 128.0 and 127.6 (C on phenyl ring), 126.9, 124.1 and 122.3 (tertiary C on terpyridyl), 104.4 (Pt−*C*≡C), 99.2 (Pt−C≡*C*), 38.1 and 37.1 (quaternary C on *tert*-butyl group), 30.7 and 30.3 ppm (primary C on *tert*-butyl group); IR (KBr): $\tilde{\nu} = 2118\ cm^{-1}$ (C≡C); FAB-MS (+ve): *m/z*: 697 $[M-ClO_4]^+$; elemental analysis calcd (%) for $C_{35}H_{40}ClN_3O_4Pt$: C 52.73, H 5.06, N 5.27; found: C 52.62, H 5.00, N 5.21.

[(*t*Bu$_3$tpy)Pt−(C≡C−1,2-C$_6$H$_4$)$_2$−C≡CC$_6$H$_5$]ClO$_4$ (9): Yield, 83%; ^1H NMR (400 MHz, CD_3CN, 25°C): $\delta = 8.91$ (d with Pt satellites, $^3J = 6.0$ Hz, 2H; terpyridyl H), 8.15 (s, 2H; terpyridyl H), 8.07 (d, $^4J = 1.7$ Hz, 2H; terpyridyl H), 7.65 (dd, $^3J = 8.2$ Hz, 1H; phenyl H), 7.59 (dd, $^3J = 7.9$ Hz, 1H; phenyl H), 7.50 (dd, $^3J = 8.1$ Hz, 1H; phenyl H),7.43–7.26 (m, 5H; phenyl H), 7.12 (m, 4H), 6.67 (m, 3H; phenyl H), 1.53 (s, 9H; *tert*-butyl H), 1.33 ppm (s, 18H; *tert*-butyl H); $^{13}C\{^1H\}$ NMR (100 MHz, CD_3CN, 25°C): $\delta = 168.1$, 167.2, 159.2 and 155.0 (quaternary C on terpyridyl), 154.7 (tertiary C on terpyridyl), 134.0, 133.4, 133.3, 133.2, 132.9, 130.3, 129.8, 129.7, 129.5, 129.0, 128.6, 127.3 and 126.5 (C on phenyl ring), 126.2 (tertiary C on terpyridyl), 126.1, 126.0 and 124.1 (C on phenyl ring), 123.8 and 122.1 (tertiary C on terpyridyl), 106.2 (Pt−*C*≡C), 102.4 (Pt−C≡*C*), 94.8 (C≡C), 91.9 (C≡C), 89.1 (C≡C), 38.1 and 36.9 (quaternary C on *tert*-butyl group), 30.7 and 30.3 ppm (primary C on *tert*-butyl group); IR (KBr): $\tilde{\nu} = 2117\ cm^{-1}$ (C≡C); FAB-MS (+ve): *m/z*: 897 $[M-ClO_4]^+$; elemental analysis calcd (%) for $C_{51}H_{48}ClN_3O_4Pt \cdot H_2O$: C 60.32, H 4.96, N 4.14; found: C 60.10, H 4.98, N 4.10.

X-ray crystallography: Single crystals of **3**·2.5 CH_3OH (slow diffusion of Et_2O into a solution of **3** in CH_3OH), **5**·CH_3CN and **6**·4 CH_3CN (slow diffusion of Et_2O into solutions of **5** or **6** in CH_3CN) were obtained. X-ray crystallographic data were collected on a MAR diffractometer with a 300 mm image plate detector using graphite-monochromated $Mo_{K\alpha}$ radiation ($\lambda = 0.71073$ Å). The crystallographic data collection parameters are summarized in Table 1. CCDC-288275 (**3**·2.5 CH_3OH), -288276 (**5**·CH_3CN), and -288277 (**6**·4 CH_3CN) contain the supplementary crystallographic data for this paper. These data can be obtained free of charge from The Cambridge Crystallographic Data Centre via www.ccdc.cam.ac.uk/data_request/cif.

Acknowledgements

This work was supported by the Areas of Excellence Scheme (AoE/P-10/01) administered by the University Grants Committee (HKSAR, China) and the Hong Kong Research Grants Council (HKU 7039/03P). W.L. thanks The University of Hong Kong for a University Postdoctoral Fellowship. We thank Dr. Rong Chen (Chemistry, HKU) and Frankie Yu-Fee Chan (EMU, HKU) for their technical assistance on TEM and thank Dr. Jie-Sheng Huang (Chemistry, HKU) for his editorial comments.

[1] a) M. A. Baldo, D. F. O'Brien, Y. You, A. Shoustikov, S. Sibley, M. E. Thompson, S. R. Forrest, *Nature* **1998**, *395*, 151–154; b) F. G. Gao, A. J. Bard, *J. Am. Chem. Soc.* **2000**, *122*, 7426–7427; c) S. Welter, K. Brunner, J. W. Hofstraat, L. De Cola, *Nature* **2003**, *421*, 54–57.

[2] a) M. H. Keefe, K. D. Benkstein, J. T. Hupp, *Coord. Chem. Rev.* **2000**, *205*, 201–228; b) J. N. Demas, B. A. DeGraff, *Coord. Chem. Rev.* **2001**, *211*, 317–351.

[3] a) P. J. Stang, F. Diederich, *Modern Acetylene Chemistry*, VCH, Weinheim, **1995**; b) J. Manna, K. D. John, M. D. Hopkins, *Adv. Organomet. Chem.* **1995**, *38*, 79–154; c) W. Lu, B. X. Mi, M. C. W. Chan, Z. Hui, C. M. Che, N. Zhu, S. T. Lee, *J. Am. Chem. Soc.* **2004**, *126*, 4958–4971; d) H. Y. Chao, W. Lu, Y. Li, M. C. W. Chan, C. M. Che, K. K. Cheung, N. Zhu, *J. Am. Chem. Soc.* **2002**, *124*, 14696–14706; e) C. Y. Wong, C. M. Che, M. C. W. Chan, J. Han, K.-H. Leung, D. L. Phillips, K. Y. Wong, N. Zhu, *J. Am. Chem. Soc.* **2005**, *127*, 13997–14007; f) K. Y. Kim, S. Liu, M. E. Köse, K. S. Schanze, *Inorg. Chem.* **2006**, *45*, 2509–2519; g) V. W. W. Yam, B. Li, Y. Yang, B. W. K. Chu, K. M. C. Wong, K. K. Cheung, *Eur. J. Inorg. Chem.* **2003**, *22*, 4035–4042.

[4] a) V. W. W. Yam, R. P. L. Tang, K. M. C. Wong, K. K. Cheung, *Organometallics* **2001**, *20*, 4476–4482; b) V. W. W. Yam, K. M. C. Wong, N. Zhu, *Angew. Chem.* **2003**, *115*, 1438–1441; *Angew. Chem. Int. Ed.* **2003**, *42*, 1400–1403; c) K. M. C. Wong, W. S. Tang, B. W. K. Chu, N. Zhu, V. W. W. Yam, *Organometallics* **2004**, *23*, 3459–3465; d) Q. Z. Yang, L. Z. Wu, Z. X. Wu, L. P. Zhang, C. H. Tung, *Inorg. Chem.* **2002**, *41*, 5653–5655.

[5] a) J. A. Bailey, M. G. Hill, R. E. Marsh, V. M. Miskowski, W. P. Schaefer, H. B. Gray, *Inorg. Chem.* **1995**, *34*, 4591–4599; b) W. B. Connick, D. Geiger, R. Eisenberg, *Inorg. Chem.* **1999**, *38*, 3264–3265; c) H. K. Yip, L. K. Cheng, K. K. Cheung, C. M. Che, *J. Chem. Soc. Dalton Trans.* **1993**, 2933–2938; d) V. W. W. Yam, K. H. Y. Chan, K. M. C. Wong, N. Zhu, *Chem. Eur. J.* **2005**, *11*, 4535–4543; e) V. W. W. Yam, K. M. C. Wong, N. Zhu, *J. Am. Chem. Soc.* **2002**, *124*, 6506–6507; f) V. W. W. Yam, K. H.-Y. Chan, K. M. C. Wong, B. W. K. Chu, *Angew. Chem.* **2006**, *118*, 6315–6319; *Angew. Chem. Int. Ed.* **2006**, *45*, 6169–6173.

[6] a) F. Camerel, R. Ziessel, B. Donnio, C. Bourgogne, D. Guillon, M. Schmutz, C. Iacovita, J. P. Bucher, *Angew. Chem.* **2007**, *119*, 2713–2716; *Angew. Chem. Int. Ed.* **2007**, *46*, 2659–2662; b) A. Y. Y. Tam, K. M. C. Wong, G. X. Wang, V. W. W. Yam, *Chem. Commun.* **2007**, 2028–2030; c) W. Lu, Y. C. Law, J. Han, S. S. Y. Chui, D. L Ma, N. Y. Zhu, C. M. Che, *Chem. Asian J.* **2008**, *3*, 59–69.

[7] a) J. M. Tour, *Chem. Rev.* **1996**, *96*, 537–554; b) J. S. Moore, *Acc. Chem. Res.* **1997**, *30*, 402–413; c) U. H. F. Bunz, *Chem. Rev.* **2000**, *100*, 1605–1644; d) U. H. F. Bunz, *Acc. Chem. Res.* **2001**, *34*, 998–1010.

[8] a) R. H. Grubbs, D. Kratz, *Chem. Ber.* **1993**, *126*, 149–157; b) R. B. Prince, J. G. Saven, P. G. Wolynes, J. S. Moore, *J. Am. Chem. Soc.* **1999**, *121*, 3114–3121.

[9] a) J. C. Nelson, J. G. Saven, J. S. Moore, P. G. Wolynes, *Science* **1997**, *277*, 1793–1796; b) L. Arnt, G. N. Tew, *J. Am. Chem. Soc.* **2002**, *124*, 7664–7665; c) R. B. Prince, L. Brunsveld, E. W. Meijer, J. S. Moore, *Angew. Chem.* **2000**, *112*, 234–236; *Angew. Chem. Int. Ed.* **2000**, *39*, 228–230; d) Y. Ishitsuka, L. Arnt, J. Majewski, S. Frey, M. Ratajczek, K. Kjaer, G. N. Tew, K. Y. C. Lee, *J. Am. Chem. Soc.* **2006**, *128*, 13123–13129; e) S. Shotwell, P. M. Windscheif, M. D. Smith, U. H. F. Bunz, *Org. Lett.* **2004**, *6*, 4151–4154; f) T. V. Jones, M. M. Slutsky, R. Laos, T. F. A. de Greef, G. N. Tew, *J. Am. Chem. Soc.* **2005**, *127*, 17235–17240; g) M. M. Slutsky, J. S. Phillip, G. N. Tew, *New J. Chem.* **2008**, *32*, 670–675; h) T. V. Jones, M. M. Slutsky, G. N. Tew, *New J. Chem.* **2008**, *32*, 676–679.

[10] a) P. Nguyen, P. Gomez-Elipe, I. Manners, *Chem. Rev.* **1999**, *99*, 1515–1548; b) R. D'Amato, I. Fratoddi, A. Cappotto, P. Altamura, M. Delfini, C. Bianchetti, A. Bolasco, G. Polzonetti, M. V. Russo, *Organometallics* **2004**, *23*, 2860–2869; c) H. B. Yang, K. Ghosh, N. Das, P. J. Stang, *Org. Lett.* **2006**, *8*, 3991–3994; d) K. Onitsuka, S. Yamamoto, S. Takahashi, *Angew. Chem.* **1999**, *111*, 129–131; *Angew. Chem. Int. Ed.* **1999**, *38*, 174–176; e) C. A. Johnson II, M. M. Haley, E. Rather, F. Han, T. J. R. Weakley, *Organometallics* **2005**, *24*, 1161–1172.

[11] D. J. Hill, M. J. Mio, R. B. Prince, T. S. Hughes, J. S. Moore, *Chem. Rev.* **2001**, *101*, 3893–4011.

[12] K. P. Baldwin, R. S. Simons, D. A. Scheiman, R. Lattimer, C. A. Tessier, W. J. Youngs, *J. Chem. Crystallogr.* **1998**, *28*, 353–360.

[13] a) B. Manimaran, P. Thanasekaran, T. Rajendran, R. J. Lin, I. J. Chang, G. H. Lee, S. M. Peng, S. Rajagopal, K. L. Lu, *Inorg. Chem.* **2002**, *41*, 5323–5325; b) J. Luo, Z. Xie, J. W. Y. Lam, L. Cheng, H. Chen, C. Qiu, H. S. Kwok, X. Zhan, Y. Liu, D. Zhu, B. Z. Tang, *Chem. Commun.* **2001**, 1740–1741; c) B. K. An, S. K. Kwon, S. D. Jung, S. Y. Park, *J. Am. Chem. Soc.* **2002**, *124*, 14410–14415.

[14] a) A. Gourdon, J.-P. Launay, *Inorg. Chem.* **1998**, *37*, 5336–5341; b) S. H. Toma, M. Uemi, S. Nikolaou, D. M. Tomazela, M. N. Eberlin, H. E. Toma, *Inorg. Chem.* **2004**, *43*, 3521–3527.

[15] a) T. A. Zeidan, S. V. Kovalenko, M. Manoharan, I. V. Alabugin, *J. Org. Chem.* **2006**, *71*, 962–975; b) R. Diercks, K. P. C. Vollhardt, *Angew. Chem.* **1986**, *98*, 268–270; *Angew. Chem. Int. Ed. Engl.* **1986**, *25*, 266–268; c) K. P. Baldwin, J. D. Bradshaw, C. A. Tessier, W. J. Youngs, *Synlett* **1993**, 853–855.

Received: March 4, 2008
Revised: July 9, 2008
Published online: September 24, 2008

